Journal of Visualization, Vol. 5, No. 3 (2002) 285-292

3D Imaging of Evaporating Fuel Droplets by Stereoscopic PIV

Palero, V.*1 and Ikeda, Y.*2

*1 Department of Applied Physics, University of Zaragoza, Pedro Cerbuna, 12, Zaragoza 50009, Spain.
*2 Department of Mechanical Engineering, Kobe University, Rokkodai 1-1, Nada, Kobe 657-8501, Japan.

Received 30 December 2001.
Revised 25 March 2002.

***Abstract*:** A gun-type burner is a widely used oil burner for industrial and domestic applications. The oil is pressure-atomized and mixed with air generating a recirculating, swirling flow. Because of the surrounding flame, fuel droplets evaporate, being difficult to obtain information on droplets' dynamics. Several laser techniques have been applied to this burner for spray diagnosis. PDA provides information about droplet size and velocity but can say little about the instantaneous spatial structures in the flow. Planar laser techniques as PIV can describe the 2D instantaneous spatial structures, but cannot provide information about the 3D structures in the flow. Then Stereoscopic PIV was applied. This technique allows us to measure the full 3D velocity vector map in a whole fluid plane. This paper has a double purpose. Firstly, to visualize the 3D structures which are present in the burner; secondly, to show that Stereoscopic PIV is an applicable technique for the diagnosis of an evaporating spray.

***Keywords*:** Stereoscopic PIV, 3D PIV, spray combustion, droplet dynamics.

1. Introduction

The spray dynamics and its interaction with a combusting turbulent airflow is an essential subject in spray combustion research (Chigier, 1976; Williams, 1985; Kuo, 1996). Many physical characteristics in spray combustion can be explained by studying the droplet break-up mechanisms, droplet evaporation, turbulent interaction, and so on.

A gun-type burner is a widely used oil burner for industrial and domestic applications. The oil is pressure-atomized and mixed with air, generating a recirculating, swirling flow. Droplet behaviour in a gun-type burner was described by size-classified PDA measurements (Kawahara et al., 1996), finding that droplets smaller than 30 μm followed the airflow, while droplets bigger than 50 μm penetrated the airflow due to their large momentum.

However, PDA is a point-measurement technique and it is hard to gain insight into the instantaneous spatial structures that appear in the flow. Recently, planar laser techniques have been adapted to combusting sprays with very good results (Hanson, 1986). Particle Image Velocimetry (PIV) has been widely used for the measurement of the two in-plane velocity components in a fluid plane (Grant, 1997). In particular, it has been applied for the study of turbulent reacting flows (Muñiz et al., 1997), showing reliability and good performance. PIV has been applied to a gun-type burner (Ikeda et al., 1999) as well. The PIV results were compared with PDA measurement results, finding that optimised PIV optics is able to detect the velocity of medium size droplets (20-50 μm).

Since the flow field in a gun-type burner is three-dimensional, it is essential to know the swirl component. Then Stereoscopic PIV has to be applied. This technique is an extension of the classical PIV, in which the fluid plane is visualized from two directions simultaneously. The differences between these two projections permit us to extract the out-of-plane component. Stereoscopic PIV has been successfully applied to air (Willert, 1997) and

liquid flows (Prasad and Adrian, 1993; Palero et al., 2000a), and also in reacting conditions for the study of a lifted flame (Han et al., 2000). Stereoscopic PIV has been applied to the gun type burner (Palero et al., 2000 b, c) and the results were compared with PDA data, finding that Stereoscopic PIV is a technique with a great potential for the analysis of complex flows.

Although this is a two-phase flow, the present work is focused on the analysis of the disperse phase (the liquid spray droplets) with a double purpose. In the first place, to visualize the 3D structures present in a gun-type burner; in the second, to demonstrate that Stereoscopic PIV is an applicable technique for spray characterization in a reacting flow in spite of the adverse measurement conditions, as evaporating droplets and the presence of soot. There are many parameters involved in a Stereoscopic PIV measurement that need to be optimised in order to improve the accuracy of the results. However, this task is beyond the scope of this work and will be done in future works.

2. Experimental Apparatus

2.1 Experimental Set-up

The gun-type burner (Fig. 1) is an oil burner available commercially for rather small (0.1 MW class) industrial furnaces and boilers. The burner specifications are listed in Table 1 and a detailed description is given in Ikeda et al. (1995). Heavy oil (type A, Japanese Industrial Standard) is pressurized to 0.7 MPa and a hollow cone spray is produced with a 60° included angle. A baffle plate acts as a flame holder and aids in reducing soot formation. The swirling flow enhances the turbulent mixing of fuel and air, and stabilizes the flame. The airflow was not seeded as only the disperse phase was analyzed.

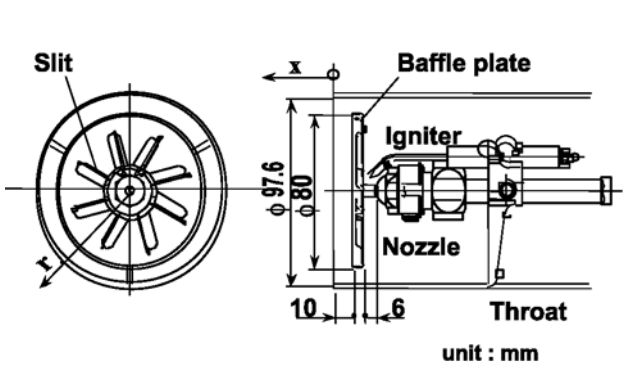

Fig. 1. Gun-type burner.

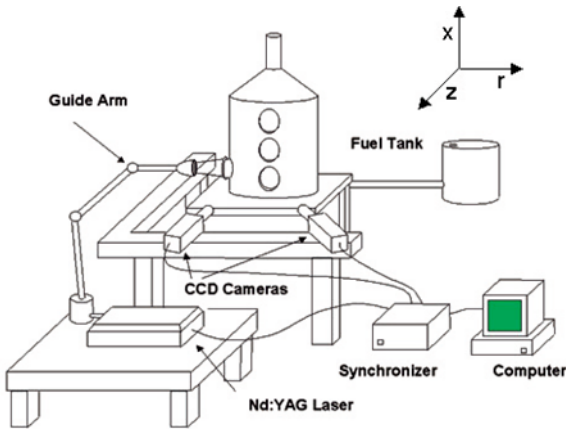

Fig. 2. Experimental set-up.

Table 1. Burner specifications.

Fuel consumption	9.45×10^{-3} (m³/h)	O_2	4.7 (vol%)
Power	0.103 MW	CO_2	10.8 (vol%)
Excess air ratio	1.2	CO	0.0 (ppm)
		NO	58.4 (ppm)

The experimental set-up used for the current investigation is presented in Fig. 2. A plane is illuminated with a dual-cavity Nd:YAG laser (Spectra-Physics PIV-400, 400 mJ pulse, 532 nm). The time ΔT between the two laser pulses was kept at 25 μs. Commercial DANTEC optics was used to form a laser sheet 1 mm thick. The angular displacement method has been applied, with a stereoscopic angle of 11°, as the test rig does not allow wider angles. Two CCD cameras (TSI PIVCAM 10-30, 8 bit, cross-correlation, 1008(H) × 1018(V) pixels, Kodak ES1.0) were used with a 60 mm focal length Micro Nikkor lenses at $f\#$ = 11. Two filters were attached to each camera. A neutral filter (Kenko, ND8), that reduces the intensity of the light that reaches the CCD sensor in a 12.5%, and an interferential filter (High Technology, center λ = 532 nm, half bandwidth: 2.76 nm), designed for selecting the light scattered by the droplets corresponding to the laser wavelength, which is 532 nm.

2.2 Flow Visualization

A direct picture of the flame produced by the burner is shown in Fig. 3. It is possible to distinguish three main regions. From top to bottom: (top) the main combustion region containing much soot luminescence; (middle) the transparent region, where the fuel droplets are evaporating; (bottom) the flame-holding region near the baffle plate.

An example of a typical stereoscopic image pair recorded in these experiments is shown in Fig. 4. Light was propagating from left to right. Stronger intensity was obtained in the camera on the right, as forward scattering is stronger than backward scattering. The unburned droplets can be distinguished in the central zone, while the sides and the recirculation regions present strong luminescence coming from soot particles and the evaporating droplets. It was assumed that the initial droplet distribution was the same as in non-reacting conditions (Kawahara et al., 1996). As the droplets move inside the flame, their sizes will change due to the evaporation. In general, it is possible to have good measurements of the unburned droplets' velocity. In the recirculation zones, the role of the soot will be important, as it will be explained later.

Fig. 3. Direct image of the flame.

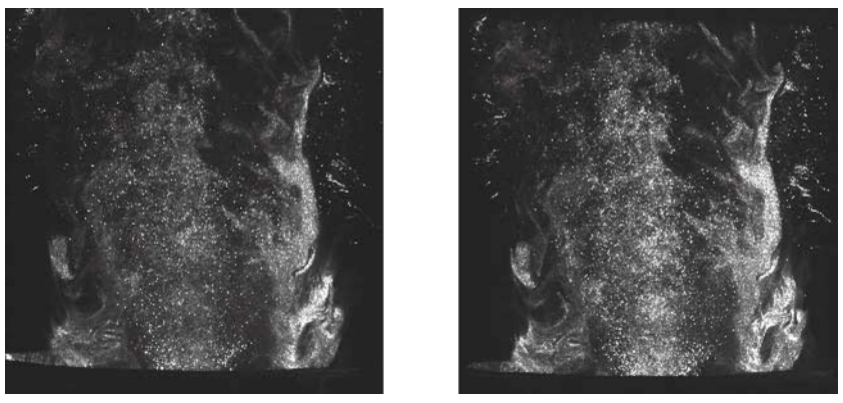

Fig. 4. Stereoscopic PIV image pair.

2.3 Image Post-processing

As the angular configuration was used, the Scheimpflug condition had to be applied in order to have the image plane in focus. However, the Scheimpflug camera arrangement introduces perspective distortion to the images. Since the image magnification is not uniform, a complex mapping function is required to map points from the fluid to the image planes correctly. Normally, a set of polynomial equations is used (Soloff et al., 1997). A calibration procedure is required to measure and correct the perspective distortion (Bjorkquist, 1998). The viewed area was 90 $\times$ 84 mm^2 (spatial resolution of 11.3 pixels/mm in the radial, and 12 pixels/mm in the axial direction). In order to measure the whole volume, the burner was displaced perpendicularly to the laser sheet. Seventeen planes were recorded from $z = -40$ mm to $z = 40$ mm every 5 mm. 450 image pairs were recorded on each plane.

A PC with two frame-grabbers captured and processed the images that were analyzed using the cross-correlated sub-regions of frame-straddled images (Insight software, version 3.00, TSI Inc). 3D vector maps were computed by interpolating the two 2D vector fields in a new grid created to define the locations where the 3D velocity was desired (Insight manual). The 3D-grid spacing was 2 mm, some 45 × 45 vectors were interpolated from 60 × 60 measured vectors on each stereoscopic image (interrogation area: 32 × 32 pixels, 50% overlap). Several factors have to be considered for the elimination of the spurious vectors. Firstly, the velocity ranges from 0 m/s to 25 m/s. Since the software does not allow setting local validation criteria, these have to be quite general in order to avoid the elimination of correctly measured vectors. On the other hand, we are studying the turbulent interaction between the spray droplets and the airflow. Then, we refused to use smoothing or any other algorithm that would improve the appearance of the instantaneous velocity vector maps but somehow would mask the real velocity. Two validation criteria were applied and the spurious vectors were eliminated using first, a range filter (the vector can not exceed reasonable limits in the displacement) and second, the vector value has to be similar to the mean value of the nearest neighboring vectors (Keane and Adrian, 1990). Every vector was compared with the mean vector obtained after averaging the 3 × 3 surrounding vectors. If the difference between the mean and the measured vector was bigger than 20%, the measured vector was eliminated and a new value was interpolated from the 3 × 3 surrounding vectors. After the validation criteria were applied, less than 8% of the measured vectors were eliminated.

3. Results and Discussion

Before analyzing the results, let us discuss the accuracy of the present experiments. The accuracy of the in-plane components is given by the minimum displacement that can be measured. In general, algorithms used in PIV can achieve an accuracy of 0.1 pixels. For an average spatial resolution of 85.5 μm/pixel, the minimum displacement detected will be 8.55 μm. As the time between exposures was kept at 25 μs, the minimum in-plane velocity measured would be 0.34 m/s, assuming uniform velocity through the window.

The accuracy of the out-of-plane component can be calculated from Lawson and Wu (1997a). These authors defined the theoretical error ratio as $e_r = d(Dz)/d(Dx)$, where Dz and Dx are the displacements in the out and in-plane directions respectively. Here, a stereoscopic angle of 11° has been used, due to the limitation imposed by the test rig. For $a = 11^\circ$ the expected error ratio would be $e_r \approx 5$. Then the accuracy on the measured out-of-plane component will be ~1.7 m/s, much lower than we would have liked. However, the same authors also defined the experimental error ratio as $e_r = d_{rms}(Dz)/d_{rms}(Dx)$ (Lawson and Wu, 1997b). This error ratio is represented in Fig. 5 for $(x, z) = (10, 0)$ mm and $(x, z) = (20, 0)$ mm. It can be seen that, in average, the error obtained for the out-of-plane component is three times bigger than the error obtained for the radial component, and twice as big as the

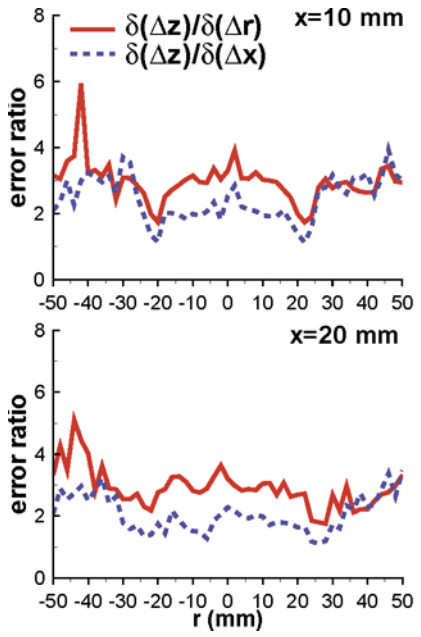

Fig. 5. Experimental error ratio.

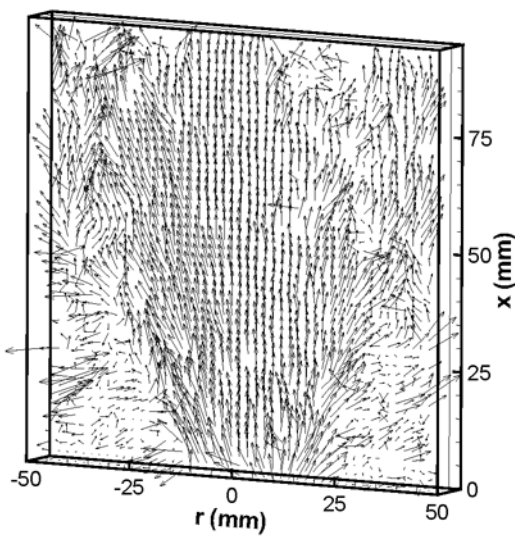

Fig. 6. Instantaneous velocity vector map.

error for the axial component. For $|r| > 30$ mm the error ratio increases, due to the lack of droplets and soot particles, as it can be seen in Fig. 4. In general, the experimental error ratio is smaller than the theoretical error predicted by Lawson and Wu (1997b). The reason is that here the Scheimpflug condition was applied, achieving sharp focused images. Also, the *f*# could be reduced, then the working conditions were similar to the measuring conditions in classical PIV.

An example of the typical instantaneous velocity vector map, obtained before any validation criterion was applied, in $z = 0$ mm is presented in Fig. 6. The spray cone structure can be seen, and three areas can be distinguished. In the central region, the droplets are moving upwards with high axial component and the three-velocity components are measured with the smallest fluctuation (rms).

Finally, we can distinguish the recirculation areas close to the baffle plate. The recirculation zones play an essential role in the flame stabilization as the airflow is entering and mixing with the evaporating droplets. There, turbulent activity can be observed as well as the formation of vortices (Palero et al., 2000c). The measurement in these zones is especially difficult as there is a mixture of soot and small (evaporating) droplets. However, the soot particles are moving as well. Due to their small size (in the order of the nm) the soot particles are acting as 'tracers', following the airflow, and therefore, providing information about its velocity. As the soot is not uniformly distributed, spurious vectors will be obtained in the points without information coming either from soot or droplets. Unfortunately, when PIV is applied, it is not possible to know the velocity corresponding to particles with different sizes. PIV should be combined with another technique that allows size discrimination such as Multi-Intensity PIV (Palero and Ikeda, 2002).

For the visualisation of the 3D structures in the spray, the iso-surfaces of the three velocity components have been calculated. 450 instantaneous velocity vector maps have been averaged on each plane. Important fluctuations were detected when less than 200 maps are averaged. However, values converge as the number of averaged maps increases. The average maps have been interpolated into a cylindrical volume and the iso-component surfaces have been extracted, using the software Tecplot ver. 7.5. In order to have the best visualization of the structures in the flow, the spatial orientation has been set different for each case.

The analysis of the iso-surfaces obtained for each velocity component can help us understand the evolution of the spray droplets in the flame. Let us start analysing the iso-surfaces for the axial component (Fig. 7). Firstly, it can be seen that the recirculation zone is forming a ring of which medium radius is 25 mm and medium height, 20 mm. Then, the dimensions and geometry of the burner are directly related with the size and shape of recirculation zone, which is an annular structure of radius half of the burner's radius.

The maximum initial droplet velocity ranges from ~15 m/s in the central region up to ~20 m/s in the shear flow region. Droplets will decelerate quickly (from 20 m/s to 13 m/s) and a large velocity gradient is observed as a consequence of the interaction with the airflow coming from the burner throat. It is possible to see that these structures are concentric and asymmetric. For the highest values (Fig. 7 (a), V_x = 17 m/s) more penetration can be observed on the left side. This is due to a misalignment between the nozzle and the baffle plate.

Droplets moving in the spray central axis kept high velocity even at large distances from the nozzle (~40 mm)

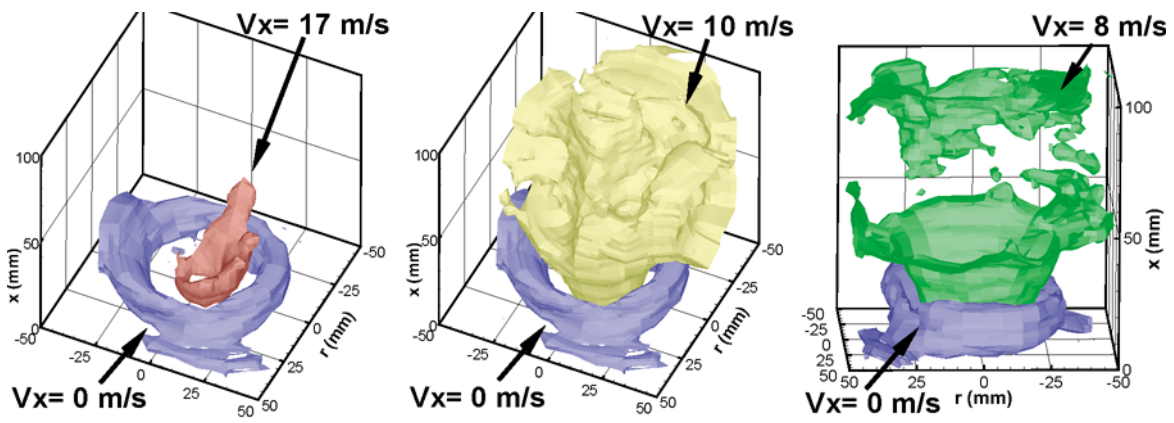

Fig. 7. Iso-surfaces for the axial velocity component.

due to the heat release and thermal expansion. For V_x = 10 m/s, a big structure is distinguished. It is a hollow, irregular structure and presents different branches; some of those are spreading across the shear flow region. Another branch is observed going vertically across the central region. This iso-component surface is covering mainly the evaporating region of the flame and it is the minimum value of the axial component measured in this zone (Fig. 7 (c)). There, the iso-surface for V_x = 8 m/s has been represented. A clear separation is obtained between the area surrounding the recirculation zone and the upper combusting region. Droplets with an initial velocity smaller than 15 m/s will almost completely evaporate after travelling some 40 mm in the flame. The typical scale for combustion is of the order of a few milliseconds for fuel droplets, assuming a d^2 law for evaporation. Droplets with high velocity will cross the evaporation region, losing part of their mass. Then, it is not possible to measure any velocity smaller than 10 m/s there, because all the slow droplets will evaporate by then. From these graphics it can be seen that the evaporating region covers approximately from $x \approx 45$ mm up to $x \approx 85$ mm.

The iso-surfaces for the radial component are shown in Fig. 8. The structures are also concentric and more penetration is measured on the left side. Again, the values of the radial component decrease from the shear flow region towards the central and recirculation zones.

The results obtained for the swirl component are shown in Fig. 9, where the iso-surfaces for a swirl of 2 m/s are represented. Two differentiated structures can be distinguished in the centre of the burner. They correspond to the spray droplets that are coming from the nozzle and have strong swirl. The maximum swirl component has a

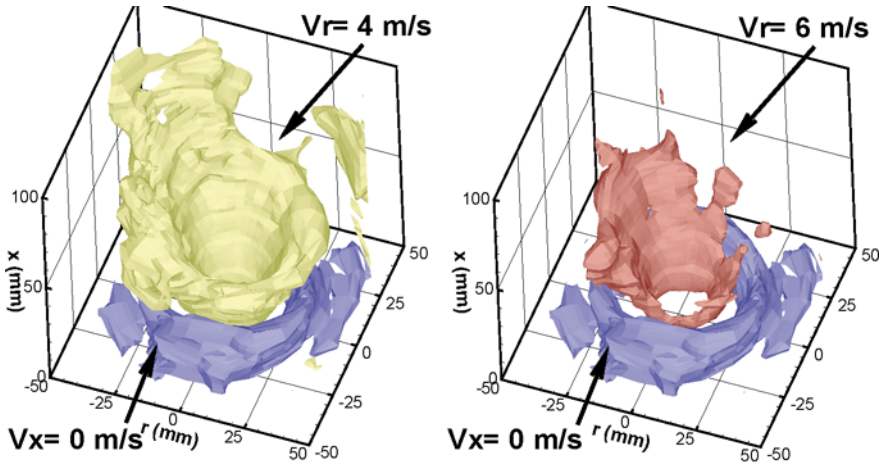

Fig. 8. Iso-surfaces for the radial velocity component.

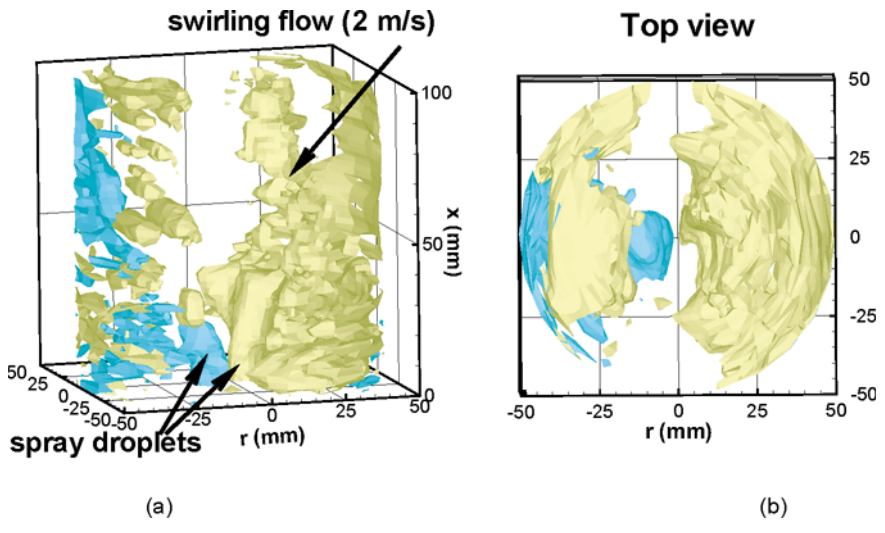

Fig. 9. Iso-surfaces for the swirl velocity component.

value of 4 m/s and is reached in a very small region close to the baffle plate. Then the swirl decreases quickly as droplets move upwards. Some asymmetry is observed in this component too, but now lower swirl values are obtained in the regions where the axial and radial component show higher penetration. On the burner's sides some swirling movement is measured as well. These structures correspond to the soot and small droplets that are following the airflow.

4. Conclusions and Future Work

Stereoscopic PIV has been applied for the visualization and study of the 3D structures of an evaporating spray in a gun-type burner, working in reacting conditions. Different concentric structures can be distinguished for the three-velocity components. The recirculation zone is an annular structure with a radius of 25 mm. This radius is half of the burner's radius, which indicates a clear dependence between the geometry of the burner and the formation of the recirculation zone. The evaporating region can be located between $x \approx 45$ mm up to $x \approx 85$ mm, and the minimum axial component measured is 10 m/s. In the shear flow region, droplets decelerate quickly as they travel upwards due to a loss in their mass because of evaporation. For the swirl component it is possible to distinguish between the swirl of the soot and evaporating droplets due to the interaction with the airflow coming from the burner throat and the three-dimensional movement of the droplets coming from the nozzle.

As future work, we intend to analyse the influence of the different parameters involved in the Stereoscopic PIV measurement and to optimise the most important ones in order to improve the accuracy of the technique.

References

Bjorkquist, D. C., Design and Calibration of a Stereoscopic PIV System, Proc. 9th Int. Symp. on Applic. of Laser Tech. to Fluid Mechanics (Lisbon), (1998).

Chigier N. A., The Atomization and Burning of Liquid Fuel Sprays, Energy and Combustion Science (1976), Pergamon International Library.

Grant, I., Particle Image Velocimetry: a Review, Proc. Inst. Mech. Eng., 211 (part C) (1997), 55-76, Journal of Mechanical Engineering Science.

Han, D., Su, L. K., Menon, R. K. and Mungal, M. G., Study of a Lifted-jet Flame Using a Stereoscopic PIV System, Proc. 10th Int. Symp. on Applic. of Laser Tech. to Fluid Mechanics (Lisbon), (2000).

Hanson, R. K., Combustion Diagnostics: Planar Imaging Techniques, Proc. Comb. Inst., 21 (1986), 1677-91, The Combustion Institute, Pittsburgh.

Ikeda, Y., Kawahara, N. and Nakajima, T., Meas. Sci. Technol., 6 (1995), 826-832.

Ikeda, Y., Yamada, N. and Nakajima, T., Spatial Structure of a Combusting Spray by PIV, Proc. 1st Int. Symp. of Turbulence and Shear Flow Phenomena (Santa Barbara), (1999).

Kawahara, N., Ikeda, Y., Hirohata, T. and Nakajima, T., Size-classified Droplets Dynamics of Combusting Spray in 0.1 MW Oil Furnace, Proc. 8th Symp. on Applic. of Laser Techniques to Fluid Mech. (Lisbon), (1996).

Keane, R. D. and Adrian, R. J., Optimization of Particle Image Velocimeters, Part I: Double-pulsed Systems, Meas. Sci. Technol, 1 (1990), 1202-1215.

Kuo, K. K., Recent Advances in Spray Combustion: Spray Atomization and Drop Burning Phenomena, Vol. I (1996), AIAA.

Lawson, N. J. and Wu, J., Three-dimensional Particle Image Velocimetry: Error Analysis of Stereoscopic Techniques, Meas. Sci. Technol., 8 (1997a), 894-900.

Lawson, N. J. and Wu, J., Three-dimensional Particle Image Velocimetry: Experimental Error Analysis of a Digital Angular Stereoscopic System, Meas. Sci. Technol., 8 (1997b), 1455-1464.

Muñiz, L., Martínez, R. E. and Mungal, M. G., Application of PIV to Turbulent Reacting Flows, Developments in Laser Techniques and Fluid Mechanics (1997), 411-424, Springer-Verlag, Berlin-Heidelberger.

Palero, V., Andrés, N., Arroyo, M. P. and Quintanilla, M., Holographic Interferometry vs Stereoscopic PIV for Measuring Out-of-plane Fields in Confined Flows, Meas. Sci. Technol , 11 (2000a), 655-66

Palero, V., Ikeda, Y., Nakajima, T. and Shakal, J., Comparison of PIV and SPIV in Application to Industrial Spray Burner, Proc. 10th Symp. on Applic. of Laser Techniques to Fluid Mech. (Lisbon), (2000b).

Palero, V., Sato, K., Ikeda, Y., Nakajima, T. and Shakal, J., Stereoscopic PIV Application for Combusting Spray in Industrial Furnaces Evaluation in a Spray, Proc. 9th Int. Symp. on Flow Visualization (Edinburgh), (2000c).

Palero, V. and Ikeda, Y., Droplet-size-classified Stereoscopic-PIV for Spray Characterization, to appear in Meas. Sci. and Technol (2002).

Prasad, A. K. and Adrian, R. J., Stereoscopic Particle Image Velocimetry Applied to Liquid Flows, Exp. Fluids, 15 (1993), 49-60.

Soloff, S. M., Adrian, R. J. and Liu, Z. C., Distortion Compensation for Generalized Stereoscopic Particle Image Velocimetry, Meas. Sci. and Technol., 8 (1997), 1441-54

Willert, C., Stereoscopic Digital Particle Image Velocimetry for Application in Wind Tunnel Flows, Meas. Sci. Technol., 8 (1997), 1465-79

Williams, F. A., Combustion Theory (1985), Addison Wesley.

Author Profile

Virginia R. Palero: She is an Assistant Professor in the Department of Applied Physics at the University of Zaragoza, Spain. She obtained her Ph. D degree from the University of Zaragoza in 1998. From 1999 to 2001 she was a post-doctoral fellow in the Department of Mechanical Engineering at Kobe University. Her research includes the development and application of laser diagnostic techniques to fluids mechanics.

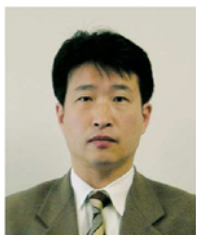

Yuji Ikeda: He is an Associate Professor in the Faculty of Engineering at Kobe University, Japan. He received his master and doctorate degrees from Kobe University in 1986 and 1989, respectively. His fields of instruction and research include combustion diagnosis, numerical analysis of turbulent flows, internal combustion engine, gas-turbine combustion among others.